INL REPORT

INL/EXT-19-55689
Unlimited Release
Printed September 2019

Sockeye Heat Pipe Theory Development: Based on the 7-Equation, Two-Phase Flow Model of RELAP-7

R.A. Berry, M. Kunick, D. Andrs, J. Hansel, R.C. Martineau
Idaho National Laboratory

Prepared by
Idaho National Laboratory
Idaho Falls, Idaho 83415

The Idaho National Laboratory is a multiprogram laboratory operated by
Battelle Energy Alliance for the United States Department of Energy
Under DOE Idaho Operations Office. Contract DE-AC07-05ID14517.

Issued by the Idaho National Laboratory, operated for the United States Department of Energy by Battelle Energy Alliance.

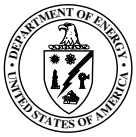

Sockeye Heat Pipe Code Theory Development: Based on the 7-Equation, Two-Phase Flow Model of RELAP-7

R.A. Berry, M. Kunick, D. Andrs, J. Hansel, R.C. Martineau

Sockeye is a MOOSE-based computer code [1] designed to simulate the thermal-hydraulic two-phase flows of heat pipes in a nuclear micro-reactor. For this application, a significantly modified version of the fully non-equilibrium, compressible, 7-equation, two-phase flow model of RELAP-7 [2] was developed. This summary report documents the significant points of this model development. It is assumed that the reader has some familiarity with RELAP-7 [2] and micro-reactor/heat pipe concepts.

A simplified schematic of a heat pipe concept is shown in the following figure.

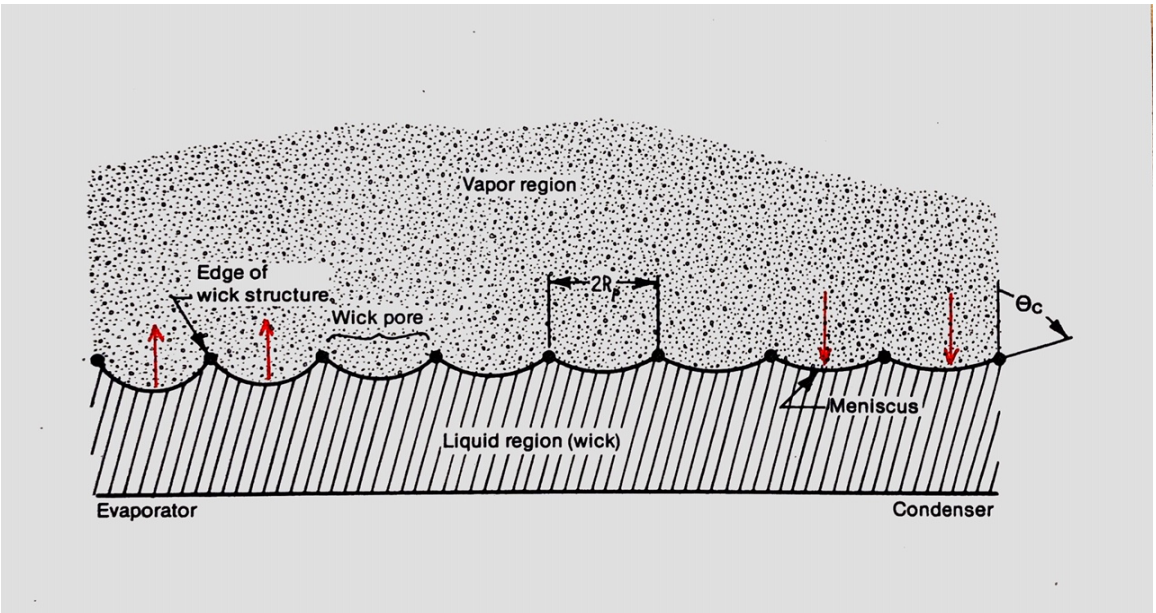

The cylindrical, coaxial geometry envisioned has the liquid coolant such as sodium flowing along the outer annular region from the condenser end to the evaporator end. At the evaporator end, the supplied heat flux causes evaporation of the liquid through the porous wick structure. Because of the mass transfer from the liquid to the vapor phase, a concave meniscus is created in the inter-pore region. The surface tension created by this concave meniscus creates a pressure gradient between the liquid and the vaporous central region. The vapor flows axially through the center region from the evaporator toward the condenser region. Heat removal from the condenser region causes the vapor to condense, filling the wick pores. This meniscus has a much larger radius of curvature so the differential pressure between the vapor and liquid is small that of the evaporator end. The net

difference between the pressure gradients at the two ends drives the circulatory flow (liquid flow from condenser to evaporator and vapor flow from evaporator to condenser).

For this problem, the analysis of surface tension effects is key. The surface tension effects modeling is similar to those used previously in the ATHENA code [3, 4]. The system will evolve with time toward an equilibrium pressure state wherein the radial pressure difference between the vapor and liquid phases is given as:

$$p_g - \frac{2\sigma}{R_c} - p_l = 0$$

where p_g and p_l are the phasic pressures of the vapor and, respectively, liquid. The term $\frac{2\sigma}{R_c}$ is the "capillary head" wherein σ is the coefficient of surface tension and R_c is the radius of curvature of the menisci. Because the interface velocity in the axial direction may be negligible, at any given axial location the dynamic evolution of the vapor volume fraction α_g due to the radial pressure difference is approximated as

$$\frac{\partial \alpha_g}{\partial t} = \mu \left(p_g - \frac{2\sigma}{R_c} - p_l \right).$$

It is assumed that the liquid-vapor meniscus is spherical, and that the maximum pressure difference that occurs across the meniscus occurs when the interface is hemispherical within the pores of the wick. When the volume of vapor per pore is within the limits corresponding to a flat or fully hemispherical interface then the phasic pressure difference can be related to the capillary head. The capillary head can be related to the vapor volume fraction as

$$\frac{2\sigma}{R_c} = \frac{2\sigma}{R_p}\left(1 - x^2\right)^{\frac{1}{2}} \quad where \quad x = \sin\theta_c \quad \left\{ \begin{array}{l} \theta_c \text{ is angle between meniscus} \\ \text{and normal to wick surface} \end{array} \right.$$

$$\alpha_g = \alpha_{g0} + N_{wp} \left\{ \frac{\pi R_p^3}{3}(2+x)\left[\frac{1-x}{(1+x)^3}\right]^{\frac{1}{2}} \right\}$$

with interfacial area per unit volume given by

$$A_{\text{int}} = \frac{2\pi R_p^2 N_{wp}}{1+x} \quad .$$

For consideration of the inversion of this equation, let us symbolically write

$$x = f\left(\alpha_g\right) \quad .$$

The analytical expression for $x = f\left(\alpha_g\right)$ is

$$x = f\left(\alpha_g\right) = \frac{1}{r} + \frac{r}{y+1} - 1$$

where

$$y = \left(\frac{3\left(\alpha_g - \alpha_{g0}\right)}{\pi R_p^3 N_{wp}} \right)^2 = \left(2+x\right)^2 \frac{\left(1-x\right)}{\left(1+x\right)^3}$$

and

$$r = \sqrt[3]{\left(y+1\right)^2 + \sqrt{y\left(1+y\left(3+y\left(3+y\right)\right)\right)}} \quad .$$

So

$$\boxed{\frac{2\sigma}{R_c} = \frac{2\sigma}{R_p}\left[1 - f^2\left(\alpha_g\right)\right]^{\frac{1}{2}}}$$

and

$$\boxed{A_{\text{int}} = \frac{2\pi R_p^2 N_{wp}}{1+f\left(\alpha_g\right)}} \quad .$$

Perhaps an easier way to view this is to define a "parameterized" vapor volume fraction $\bar{\alpha}_v$

$$\bar{\alpha}_v \equiv \left(\alpha_v - \alpha_{v0}\right)\left(\frac{3}{N_{wp}\pi r_c^3}\right) = \frac{\left(2+x\right)\left(1-x\right)^{\frac{1}{2}}}{\left(1+x\right)^{\frac{3}{2}}}$$

and a "parameterized" capillary pressure $\Delta\overline{p}_c$

$$\Delta\overline{p}_c \equiv \frac{\Delta p_c\, r_c}{2\sigma} = \left(1 - x^2\right)^{\frac{1}{2}}.$$

Then we can cross-plot $\Delta\overline{p}_c$ and $\overline{\alpha}_v$ for equally spaced values of x between 0.0 and 1.0. For 100 equally spaced increments (in x) over this interval the following plot is obtained:

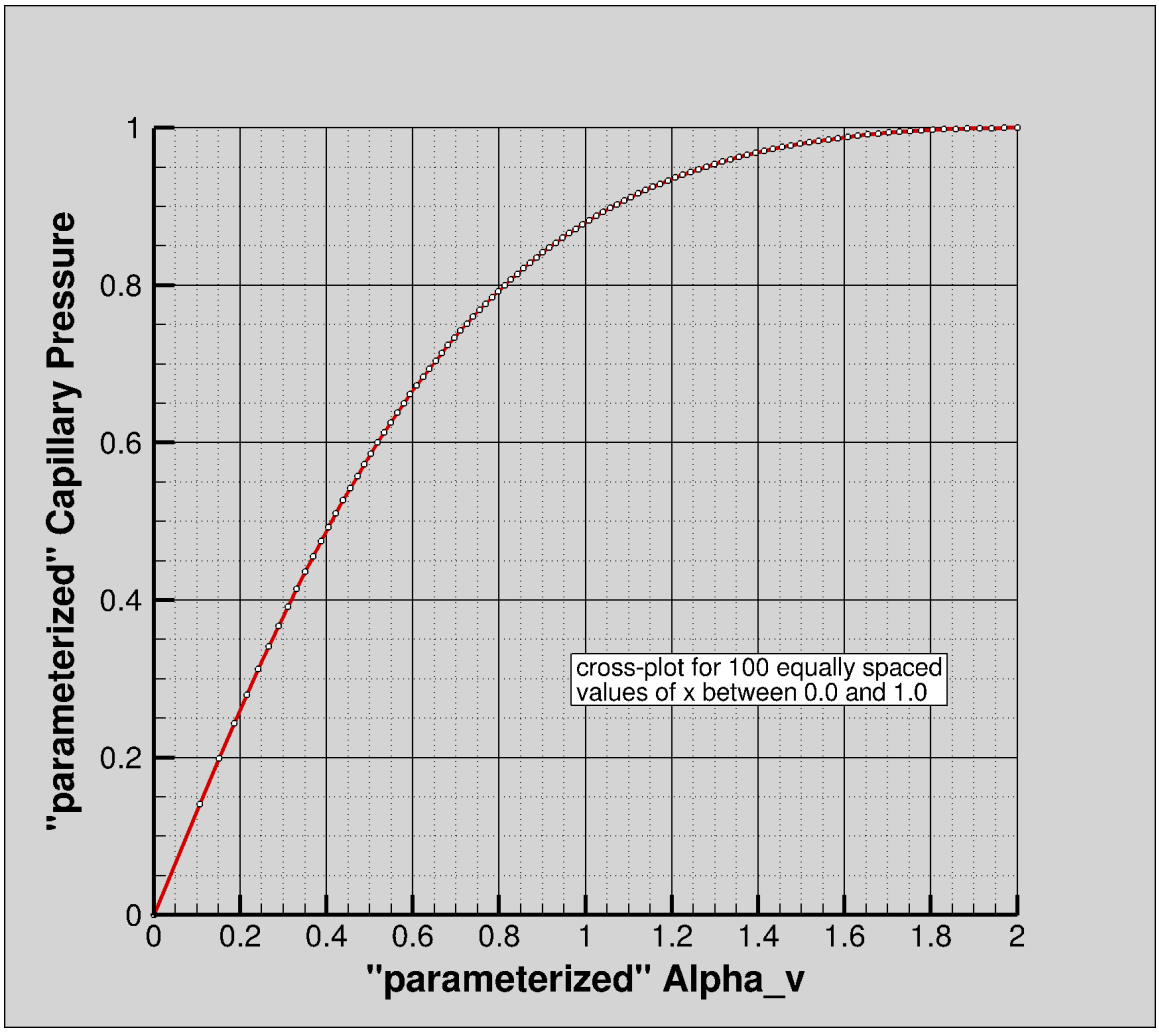

If the vapor volume lies outside of the limits (between flat meniscus and hemispherical meniscus) then the interphase pressure difference is either status quo from RELAP-7 [2] current model (or possibly zero) or at maximum according to:

$$V_c < 0 \qquad A\mu\left(p_l - p_g\right)$$

and for

$$V_c > \frac{2\pi R_p^3}{3} \qquad A\mu\left(p_l + \frac{2\sigma}{R_p} - p_g\right)$$

where

$$V_c = \frac{\pi R_p^3}{3}\left(2+x\right)\sqrt{\frac{1-x}{\left(1+x\right)^3}} \quad .$$

More options for future development of a more sophisticated wick model are included in *Appendix I*.

The heat and mass transfer coefficients at the wall, and at the liquid-vapor interface are utilized as

$$q_{wall} = h_{conv,wall} A_{wall}\left(T_{wall} - T_l\right)$$
$$q_{l,\text{int}} = h_{conv,l} A_{\text{int}}\left(T_l - T_{\text{int}}\right)$$
$$q_{g,\text{int}} = h_{conv,g} A_{\text{int}}\left(T_v - T_{\text{int}}\right)$$

$$\Gamma_{i,g} = \frac{q_{l,\text{int}} + q_{g,\text{int}}}{h_g - h_l} \quad .$$

However, a simple model results, due to the high heat transfer rates, by assuming that $T_l = T_{\text{int}}$, so

$$q_{wall,l} = \overline{h}_{conv,wall} A_{wall}\left(T_{wall} - T_l\right)$$
$$q_{g,\text{int}} = \overline{h}_{conv,g} A_{\text{int}}\left(T_g - T_l\right)$$

$$\Gamma_{i,g} = \frac{q_{wall,l} + q_{g,\text{int}}}{h_g - h_l} \quad .$$

The heat transfer coefficient between the vapor and interface/wick/liquid could be approximated with the Dittus-Boelter relation.

The compressible, 7-equation, two-phase model has independent pressures for each phase and allows full mechanical and thermodynamical non-equilibrium. It

is hyperbolic and well-posed. For stratified or annular flow the dynamic volume fraction evolution equation, and mass, momentum, and total energy equations for the ***continuous liquid phase*** are (in order):

$$\frac{\partial \alpha_l A}{\partial t} + u_{\text{int}} A \frac{\partial \alpha_l}{\partial x} = A\mu(p_l + \frac{2\sigma}{R_c} - p_g) - \frac{\Gamma_{i,g} A_{\text{int}} A}{\rho_{\text{int}}} - \frac{\Gamma_{wall,g}}{\rho_{\text{int}}}$$

$$\frac{\partial \alpha_l \rho_l A}{\partial t} + \frac{\partial \alpha_l \rho_l u_l A}{\partial x} = -\Gamma_{i,g} A_{\text{int}} A - \Gamma_{wall,g}$$

$$\begin{aligned}\frac{\partial \alpha_l \rho_l u_l A}{\partial t} + \frac{\partial \alpha_l A(\rho_l u_l^2 + p_l)}{\partial x} &= p_{\text{int}} A \frac{\partial \alpha_l}{\partial x} + p_l \alpha_l \frac{\partial A}{\partial x} + A\lambda(u_g - u_l) \\ &\quad - \Gamma_{i,g} A_{\text{int}} u_{\text{int}} A - \Gamma_{wall,g} u_{\text{int}} - F_{wall-fric,l} \\ &\quad - F_{fric,g} + \alpha_l \rho_l \vec{g} \cdot \hat{n}_{axis} A\end{aligned}$$

$$\begin{aligned}\frac{\partial \alpha_l \rho_l E_l A}{\partial t} + \frac{\partial \alpha_l u_l A(\rho_l E_l + p_l)}{\partial x} &= p_{\text{int}} u_{\text{int}} A \frac{\partial \alpha_l}{\partial x} - \overline{p}_{\text{int}} A\mu(p_l + \frac{2\sigma}{R_c} - p_g) \\ &\quad + \overline{u}_{\text{int}} A\lambda(u_g - u_l) \\ &\quad + \Gamma_{i,g} A_{\text{int}} \left(\frac{p_{\text{int}}}{\rho_{\text{int}}} - H_{l,\text{int}} \right) A \\ &\quad + A_{\text{int}} h_{conv,l} (T_{\text{int}} - T_l) A \\ &\quad + Q_{wall,l,conv} \\ &\quad - \Gamma_{wall,g} \left(h_l + \frac{1}{2} u_l^2 \right) \\ &\quad + \alpha_l \rho_l u_l \vec{g} \cdot \hat{n}_{axis} A\end{aligned}$$

Similarly, for stratified or annular flow the dynamic volume fraction evolution equation, and mass, momentum, and total energy equations for the ***continuous vapor phase*** are (in order):

$$\alpha_g = 1 - \alpha_l$$

$$\frac{\partial \alpha_g \rho_g A}{\partial t} + \frac{\partial \alpha_g \rho_g u_g A}{\partial x} = \Gamma_{i,g} A_{\text{int}} A + \Gamma_{wall,g}$$

$$\begin{aligned}\frac{\partial \alpha_g \rho_g u_g A}{\partial t} + \frac{\partial \alpha_g A(\rho_g u_g^2 + p_g)}{\partial x} &= p_{\text{int}} A \frac{\partial \alpha_g}{\partial x} + p_g \alpha_g \frac{\partial A}{\partial x} + A\lambda(u_l - u_g) \\ &\quad + \Gamma_{i,g} A_{\text{int}} u_{\text{int}} A + \Gamma_{wall,g} u_{\text{int}} - F_{wall-fric,g} \\ &\quad - F_{fric,l} + \alpha_g \rho_g \vec{g} \cdot \hat{n}_{axis} A\end{aligned}$$

$$\frac{\partial \alpha_g \rho_g E_g A}{\partial t} + \frac{\partial \alpha_g u_g A(\rho_g E_g + p_g)}{\partial x} = p_{\text{int}} u_{\text{int}} A \frac{\partial \alpha_g}{\partial x} - \overline{p}_{\text{int}} A \mu (p_g - \frac{2\sigma}{R_c} - p_l)$$
$$+ \overline{u}_{\text{int}} A \lambda (u_l - u_g)$$
$$- \Gamma_{i,g} A_{\text{int}} \left(\frac{p_{\text{int}}}{\rho_{\text{int}}} - H_{g,\text{int}} \right) A$$
$$+ A_{\text{int}} h_{conv,g} (T_{\text{int}} - T_g) A$$
$$+ Q_{wall,g}$$
$$+ \Gamma_{wall,g} \left(h_l + \frac{1}{2} u_l^2 \right) + Q_{wall,l,boil}$$
$$+ \alpha_g \rho_g u_g \vec{g} \cdot \hat{n}_{axis} A \quad .$$

The two-phase flow equations above are basically those of the RELAP-7 code [2]. The terms shown in the color cyan are those that may be removed for a heat pipe model. The capillary head term, shown in the color red, must of course be added to the basic RELAP-7 [2] equation set.

One could assume, for a first approximation, the volume fraction gradient terms are negligible in the volume fraction evolution equation, as well as in the momentum and total energy equations. Similarly, the cross-sectional area gradient terms could also be approximated as being negligible. The RELAP-7 [2] two-phase equations are again shown, in the same sequential order, with these additional negligible terms shown in cyan color (again with the added capillary head term shown in red color). For the ***continuous liquid phase***

$$\frac{\partial \alpha_l A}{\partial t} + u_{\text{int}} A \frac{\partial \alpha_l}{\partial x} = A \mu (p_l + \frac{2\sigma}{R_c} - p_g) - \frac{\Gamma_{i,g} A_{\text{int}} A}{\rho_{\text{int}}} - \frac{\Gamma_{wall,g}}{\rho_{\text{int}}}$$

$$\frac{\partial \alpha_l \rho_l A}{\partial t} + \frac{\partial \alpha_l \rho_l u_l A}{\partial x} = -\Gamma_{i,g} A_{\text{int}} A - \Gamma_{wall,g}$$

$$\frac{\partial \alpha_l \rho_l u_l A}{\partial t} + \frac{\partial \alpha_l A(\rho_l u_l^2 + p_l)}{\partial x} = p_{\text{int}} A \frac{\partial \alpha_l}{\partial x} + p_l \alpha_l \frac{\partial A}{\partial x} + A \lambda (u_g - u_l)$$
$$- \Gamma_{i,g} A_{\text{int}} u_{\text{int}} A - \Gamma_{wall,g} u_{\text{int}} - F_{wall-fric,l}$$
$$- F_{fric,g} + \alpha_l \rho_l \vec{g} \cdot \hat{n}_{axis} A$$

$$\frac{\partial \alpha_l \rho_l E_l A}{\partial t} + \frac{\partial \alpha_l u_l A(\rho_l E_l + p_l)}{\partial x} = p_{\text{int}} u_{\text{int}} A \frac{\partial \alpha_l}{\partial x} - \overline{p}_{\text{int}} A \mu (p_l + \frac{2\sigma}{R_c} - p_g)$$
$$+ \overline{u}_{\text{int}} A \lambda (u_g - u_l)$$
$$+ \Gamma_{i,g} A_{\text{int}} \left(\frac{p_{\text{int}}}{\rho_{\text{int}}} - H_{l,\text{int}} \right) A$$
$$+ A_{\text{int}} h_{conv,l} (T_{\text{int}} - T_l) A$$
$$+ Q_{wall,l,conv}$$
$$- \Gamma_{wall,g} \left(h_l + \frac{1}{2} u_l^2 \right)$$
$$+ \alpha_l \rho_l u_l \vec{g} \cdot \hat{n}_{axis} A$$

and for the ***continuous vapor phase***

$$\alpha_g = 1 - \alpha_l$$

$$\frac{\partial \alpha_g \rho_g A}{\partial t} + \frac{\partial \alpha_g \rho_g u_g A}{\partial x} = \Gamma_{i,g} A_{\text{int}} A + \Gamma_{wall,g}$$

$$\frac{\partial \alpha_g \rho_g u_g A}{\partial t} + \frac{\partial \alpha_g A(\rho_g u_g^{\,2} + p_g)}{\partial x} = p_{\text{int}} A \frac{\partial \alpha_g}{\partial x} + p_g \alpha_g \frac{\partial A}{\partial x} + A \lambda (u_l - u_g)$$
$$+ \Gamma_{i,g} A_{\text{int}} u_{\text{int}} A + \Gamma_{wall,g} u_{\text{int}} - F_{wall-fric,g}$$
$$- F_{fric,l} + \alpha_g \rho_g \vec{g} \cdot \hat{n}_{axis} A$$

$$\frac{\partial \alpha_g \rho_g E_g A}{\partial t} + \frac{\partial \alpha_g u_g A(\rho_g E_g + p_g)}{\partial x} = p_{\text{int}} u_{\text{int}} A \frac{\partial \alpha_g}{\partial x} - \overline{p}_{\text{int}} A \mu (p_g - \frac{2\sigma}{R_c} - p_l)$$
$$+ \overline{u}_{\text{int}} A \lambda (u_l - u_g)$$
$$- \Gamma_{i,g} A_{\text{int}} \left(\frac{p_{\text{int}}}{\rho_{\text{int}}} - H_{g,\text{int}} \right) A$$
$$+ A_{\text{int}} h_{conv,g} (T_{\text{int}} - T_g) A$$
$$+ Q_{wall,g}$$
$$+ \Gamma_{wall,g} \left(h_l + \frac{1}{2} u_l^2 \right) + Q_{wall,l,boil}$$
$$+ \alpha_g \rho_g u_g \vec{g} \cdot \hat{n}_{axis} A$$

.

One could also assume, for a simple model, that the liquid is blocked or "sheltered" from the velocity of the vapor by the wick structure, so that the usual interphase friction in the axial direction in the liquid phase is negligible. Instead, the

Fanning or Darcy pipe friction factor formulations could be used between the axial vapor flow and the wick and also between the axial liquid flow and the wick. Along a wall or wick surface the shear stress is given by

$$\tau = \frac{\delta F_f}{2\pi r\, dx}$$

where δF_f is the force in the axial direction and $2\pi r\, dx$ is the wall or wick surface area upon which it acts. The Fanning friction factor, f, and Darcy friction factor, f', are given, respectively, by

$$f \equiv \frac{\tau}{\frac{1}{2}\rho u^2} = \frac{\delta F_f}{\frac{1}{2}\rho u^2 \left(2\pi r\right) dx} \quad and \quad f' \equiv \frac{4\tau}{\frac{1}{2}\rho u^2} = 4f \ .$$

So the axial momentum balance for the annular liquid region is

$$\frac{\partial\left(\rho u A\right)_l}{\partial t} + \frac{\partial}{\partial x}\left[\left(\rho u^2 + p\right)A\right]_l - \left(p\frac{\partial A}{\partial x}\right)_l + \left(f_{wall} r_{wall} + f_{wick} r_{wick,\,outer}\right)\pi\left(\rho u^2\right)_l = 0$$

and the axial momentum balance for the cylindrical vapor core region is

$$\frac{\partial\left(\rho u A\right)_g}{\partial t} + \frac{\partial}{\partial x}\left[\left(\rho u^2 + p\right)A\right]_g - \left(p\frac{\partial A}{\partial x}\right)_g + f_{wick} r_{wick,\,inner}\pi\left(\rho u^2\right)_g = 0 \ .$$

Finally, the numerical finite volume method used in RELAP-7 [2] and Sockeye relies on the HLLC [5, 6] approximate Riemann solver to obtain the fluxes at each volume (or cell) interface. However, the HLLC solver, like most approximate Riemann solvers loses accuracy in the limit of low speed flow (i.e. low Mach number flow). *Appendix II* further discusses this issue and develops an all-speed modification that corrects the approximate Riemann solver for low Mach number flows, thus enabling the accurate solution for compressible flows of all speeds.

Appendix I: Future Improvements

Because the *capillary pressure depends on the new time volume fraction*, it makes sense to construct a table of values (either analytically derived or experimentally determined) and perform a fast table look-up within the numerical simulation for the capillary head term. By making certain assumptions, may be

possible to accurately speed up this search. There are several potential advantages with this approach:

- The capillary head can be modeled using experimental data collected for a specific heat pipe to give very accurate capillary effects for that heat pipe.
- The assumption that the radii of the wick pores are the same throughout the wick can be removed.
- The model can allow for the real possibility of negative capillary pressures.
- Physically real hysteresis capability (by keeping track of where the volume fraction is on the curve, e.g. if the wick is already flooded, the capillary pressure will remain zero until a vapor depression into the wick is made) can be incorporated into the model.

These potential advantages are illustrated without further (self-evident) comment in the figures below.

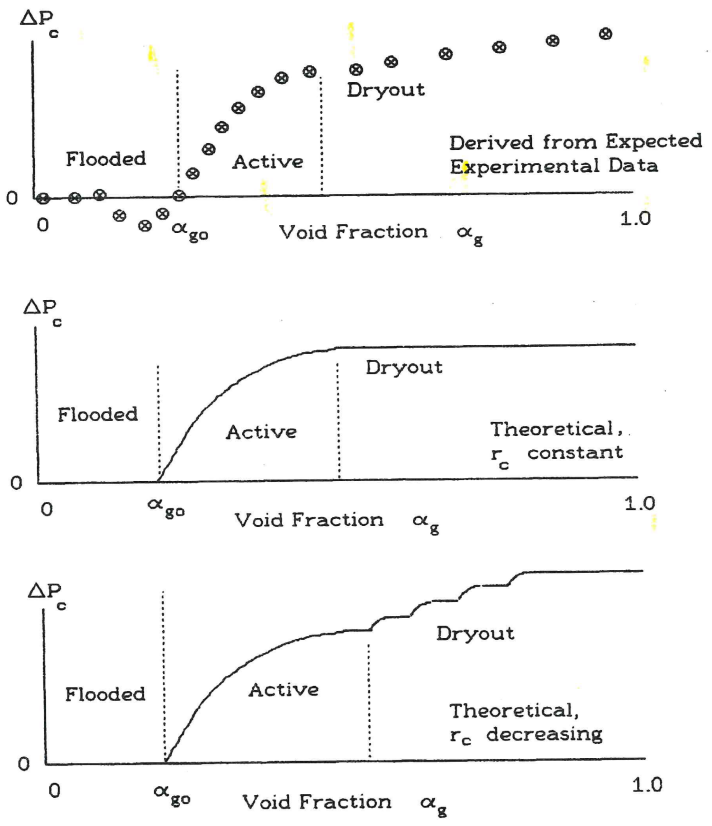

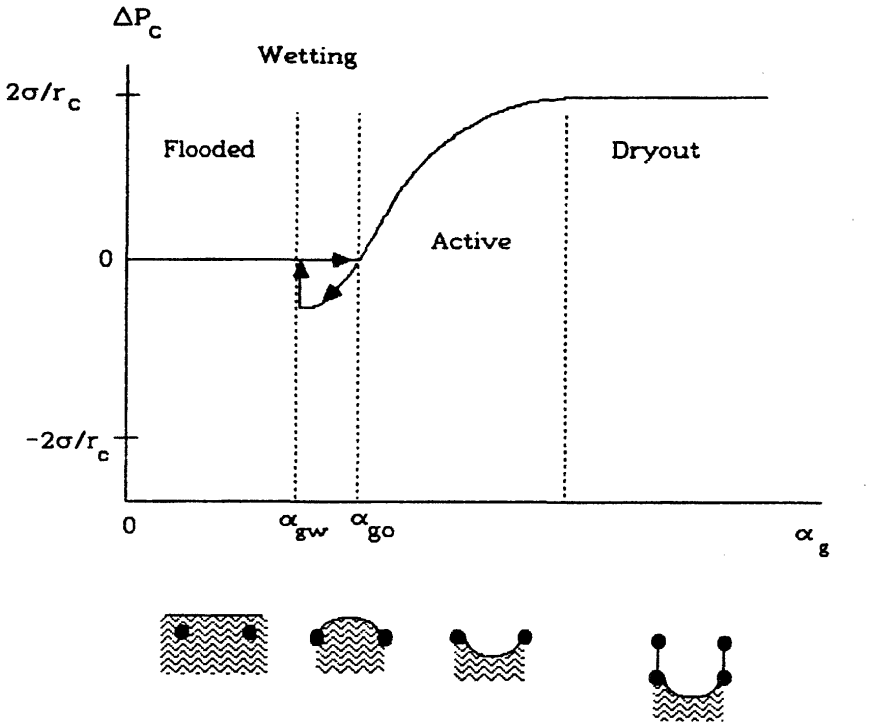

Another future improvement includes the representation of a finite-thickness wick in which a Darcy law or an Ergun drag relation approximates the frictional drag between the radial liquid/vapor flow and the stationary wick. This would augment the capillary head term in the two-phase balance equations above.

Appendix II: Simple All-Speed Modifications to the HLLC Approximate Riemann Solver

The finite volume framework now adopted in RELAP-7 [2] is well developed for the simulation of steady and unsteady compressible flows of moderate and high Mach number, as well as for the investigation of wave propagation phenomena such as sharp and accurate shock capturing in unsteady flow. Such finite volume methods for these hyperbolic problems are conservative by construction and enable efficient time dependent simulations. These finite volume methods typically rely upon Godunov type methods to compute the intercellular fluxes using approximate solutions to the intercellular Riemann problem.

Because much of the detailed information provided by a full solution of the Riemann problem is lost in the projection step of a Godunov method, it is often possible to replace the full solution by an approximate solution with little detriment on the answer. Thus there exist a plethora of Godunov type methods in the

literature that have been espoused for these types of problems [7]. For example the HLL [8] solver is an approximate Riemann solver with one intermediate state that needs as input (in addition to the initial and boundary conditions) only the lower and upper bounds, S_L and S_R, respectively, for the smallest and largest signal velocities.

However, this argument breaks down as the flow Mach number becomes small, necessitating an examination of the dissipative portion of the Godunov flux. Godunov type methods based on approximate Riemann solvers fail in the limit of low Mach number flows and require modification to overcome this low Mach number problem. Otherwise, the accuracy and the convergence of the Godunov approximation are significantly decreased if the local Mach number is in the weakly compressible regime, approximately $M \leq 0.1$. The large difference between the acoustic wave speed $|u|+c$ and the fluid flow speed u is associated with the slow convergence. We define the stiffness of the equation by the condition number C, which is in turn defined by the ratio of the largest eigenvalue of the system to the smallest one, i.e.

$$C = \frac{|u|+c}{|u|} = 1 + \frac{1}{M} \ .$$

Because the maximum time step is limited by the fastest wave speed $|u|+c$, a larger condition number (where $M \to 0$) reduces the convergence rate of the numerical scheme.

More significantly, a decrease of accuracy is associated with the incorrect estimation of the numerical dissipation in standard schemes in the low Mach number limit. This issue is linked more to the discretization of the spatial operators and insignificantly to the discretization of the time operators (and generally is not just restricted to Godunov-type schemes). This decrease of accuracy occurs for gaseous flows but is further intensified for liquids due to their large acoustic impedance. A simple example illustrates this failure. Consider a definition of the interface pressure in the Godunov approach wherein, if the variations of the state variables are smooth, any method based on compatibility relations or on Rankine-Hugoniot relations will lead roughly [7] to an interface pressure definition comparable to

$$p^* = \frac{p_L + p_R}{2} + \frac{u_L - u_R}{2} \overline{\rho} \overline{c}$$

where $\overline{\rho}$ and $\overline{c}$ are average density and speed of sound, respectively. In this equation, it is seen that the coupling of pressure with velocity is weighted (multiplied) by the acoustic impedance, $\overline{\rho} \overline{c}$, (which is approximately a constant

value if the Mach number remains small within the flow field). Moreover, the second term on the RHS of this equation adds to the numerical dissipation of the numerical scheme. It can be demonstrated that this calculated interface pressure p^* is extremely sensitive even to small variations in the velocity field (recall that the Godunov approach treats all variations as discrete jumps), making accurate calculation of numerical pressure flux difficult, especially for a smooth water flow. For example [9], consider a very simple accelerating flow with constant total pressure p_0. Assume an average sound speed of $\overline{c} = 1500 \frac{m}{sec}$ and the following left and right states:

$p_L = 1\, bar$	$p_R = 0.95\, bar$
$u_L = 10 \frac{m}{sec}$	$u_R = 10.5 \frac{m}{sec}$
$\rho_L = 1000 \frac{kg}{m^3}$	$\rho_R = 1000 \frac{kg}{m^3}$

Application of the standard p^* equation gives $p^* = -2.78\, bar$ which is obviously wrong!

Therefore, the low Mach number problem is directly related to the numerical approximation of the interface pressure p^* based on compatibility or Rankine-Hugoniot relations.

In order to overcome the low Mach number problem, a modified numerical flux is developed using an asymptotically consistent pressure flux definition, i.e.

$$p^* = \frac{\left(\rho c\right)_R p_L + \left(\rho c\right)_L p_R}{\left(\rho c\right)_L + \left(\rho c\right)_R} .$$

The velocity flux u^* is calculated in Sockeye and RELAP-7 using the HLLC approximate Riemann method [5, 6]; or, alternatively, it can be calculated as

$$u^* = \frac{\left(\rho c u\right)_L + \left(\rho c u\right)_R + p_L - p_R}{\left(\rho c\right)_L + \left(\rho c\right)_R} .$$

This interface pressure definition for p^* does not contain the coupling of pressure and velocity that causes the low Mach number problem. Though this definition for p^* is less dissipative than the standard HLLC approach, the numerical stability appears to be well preserved in simulations, leading to the conclusion that the definition of u^* evidently includes sufficient coupling of pressure and velocity.

Because the interface pressure p^* has been modified, compatible expressions for interfacial density ρ^* and interfacial specific internal energy e^* must be employed. For low Mach flows the waves are acoustic or approximately isentropic. With this assumption we approximate

$$\rho^* = \begin{cases} \rho_L + \dfrac{p^* - p_L}{c_L^2} & u^* \geq 0 \\ \rho_R + \dfrac{p^* - p_R}{c_R^2} & u^* < 0 \end{cases} .$$

For specific internal energy, a form of the Rankine-Hugoniot relations is employed which is independent of wave speed to yield

$$e^* = \begin{cases} e_L - \dfrac{p^* + p_L}{2}\left(\dfrac{1}{\rho^*} - \dfrac{1}{\rho_L}\right) & u^* \geq 0 \\ e_R - \dfrac{p^* + p_R}{2}\left(\dfrac{1}{\rho^*} - \dfrac{1}{\rho_R}\right) & u^* < 0 \end{cases} .$$

The fluxes used are then formed as a Mach number weighted function of the HLLC fluxes [5, 6] and the fluxes computed with these low Mach number interfacial values. The weighting function $w(M)$ is determined as follows. First, an interface Mach number M^* is determined,

$$M^* = \frac{M_L + M_R}{2} \quad \textit{or alternatively} \quad M^* = \max\left(M_L, M_R\right)$$

where $M_K = \dfrac{|u_K|}{c_K}$ where $K = \{L, R\}$. Then, the *weighting function* is formed

$$w(M) = \begin{cases} 0 & M^* \leq 0.1 \\ \dfrac{1}{2}M^* - \dfrac{1}{2} & 0.1 < M^* \leq 0.3 \\ 1 & M^* > 0.3 \end{cases} .$$

Finally, the weighted cell interface fluxes f can then constructed as the weighted sum of the fluxes computed with these new *-variables and the HLLC fluxes:

$$
\begin{aligned}
f(1) &= \left(1 - w\left(M^*\right)\right)\left(\rho^* u^*\right) \; + \; w\left(M^*\right) f_{HLLC}(1) \\
f(2) &= \left(1 - w\left(M^*\right)\right)\left(\rho^* u^* u^* + p^*\right) \; + \; w\left(M^*\right) f_{HLLC}(2) \\
f(3) &= \left(1 - w\left(M^*\right)\right)\left(\rho^* \left(e^* + \frac{1}{2} u^* u^*\right) u^* + p^* u^*\right) \; + \; w\left(M^*\right) f_{HLLC}(3)
\end{aligned}
\quad .
$$

References

1. D.R. Gaston, C.J. Permann, J.W. Peterson, A.E. Slaughter, D. Andrs, Y. Wang, M.P. Short, D.M. Perez, M.R. Tonks, J. Ortensi, R.C. Martineau, "Physics-Based Multiscale Coupling for Full Core Nuclear Reactor Simulation," *Annals of Nuclear Engineering* **84** (2015) 45-54.

2. R.A. Berry, L. Zou, H. Zhao, H. Zhang, J.W. Peterson, R.C. Martineau, S.Y. Kadioglu, D. Andrs, *RELAP-7 Theory Manual*, Idaho National Engineering Laboratory external report INL/EXT-14-31366, initial version February 2014, periodically updated since.

3. K.E. Carlson, P.A. Roth, V.H. Ransom, *ATHENA Code Manual Volume 1: Code Structure, System Models, and Solution Methods*, Idaho National Laboratory informal report EGG-RTH-7397, September 1986.

4. V.A. Mousseau, G.A. Mortensen, V.H. Ransom, *Heat Pipe Model for ATHENA*, Idaho National Laboratory informal report EGG-CATT-7864, September 1987.

5. E.F. Toro, "Restoration of the Contact Surface in the HLL-Riemann Solver," *Shock Waves* **4** (1994) 25-34.

6. E.F. Toro, "The HLLC Riemann Solver," *Shock Waves* (2019). Accepted, on line June 2019, https://doi.org/10.1007/s00193-019-00912-4.

7. E.F. Toro, *Riemann Solvers and Numerical Methods for Fluid Dyn*amics, 3rd Edn., Springer, Berlin (2009).

8. A. Harten, P.D. Lax, B. van Leer, "On Upstream Differencing and Godunov-type Schemes for Hyperbolic Conservation Laws," *SIAM Review* **25** (1983) 35-61.

9. I.H. Sezal, "Compressible Dynamics of Cavitating 3-D Multi-Phase Flows," genehmigten Dissertation, Technische Universität München, Lehrstuhl Für Fluidmechanik, Fachgebiet Gasdynamik, 2009.